Erfurth, S. C., Kiser, E. J., & Peticolas, W. L. (1972) *Proc. Natl. Acad. Sci. U.S.A. 69*, 938-941.
Erfurth, S. C., Bond, P. J., & Peticolas, W. L. (1975) *Biopolymers 14*, 1245-1257.
Johnston, P. D., & Rich, A. (1985) *Cell (Cambridge, Mass.) 42*, 713-724.
McClarin, J. A., Frederick, C. A., Wang, B.-C., Greene, P. J., Boyer, H. W., Grable, H. W., & Rosenberg, J. M. (1986) *Science 243*, 1526.
McLean, M. J., Blaho, J. A., Kilpatrick, M. W., & Wells, R. D. (1986) *Proc. Natl. Acad. Sci. U.S.A. 83*, 5884-5888.
Patapoff, T. W., Thomas, G. A., Wang, Y., & Peticolas, W. L. (1988) *Biopolymers 27*, 493-507.
Peticolas, W. L., Yang, W., & Thomas, G. A. (1988) *Proc. Natl. Acad. Sci. U.S.A. 85*, 2579-2583.
Ridoux, J. P., Liquier, J., & Taillandier, E. (1988) *Biochemistry 27*, 3874-3878.
Seeman, N. C., Rosenberg, J. M., & Rich, A. (1976) *Proc. Natl. Acad. Sci. U.S.A. 73*, 804-808.
Sheardy, R. D. (1988) *Nucleic Acids Res. 16*, 1153-1167.
Sheardy, R. D., & Winkle, S. A. (1989) *Biochemistry 28*, 720-725.
Singleton, C. K., Klysik, J., Stirdivant, S. M., & Wells, R. D. (1982) *J. Biol. Chem. 257*, 10159-10165.
Thamann, T. J., Lord, R. C., Wang, A. H.-J., & Rich, A. (1981) *Nucleic Acids Res. 9*, 5443-5457.
Thomas, G. A., Patapoff, T. W., Wang, Y., & Peticolas, W. L. (1987) in *Book of Abstracts, Fifth Conversation in Biomolecular Stereodynamics* (Sarma, R. H., Ed.) State University of New York at Albany, Albany, NY.
Thomas, G. A., Kubasek, W. L., Peticolas, W. L., Greene, P., Grable, J., & Rosenberg, J. M. (1989) *Biochemistry 28*, 2001-2009.
Wang, Y., Thomas, G. A., & Peticolas, W. L. (1987a) *Biochemistry 26*, 5178-5186.
Wang, Y., Thomas, G. A., & Peticolas, W. L. (1987b) *J. Biomol. Struct. Dyn. 5*, 249-274.

Three-Dimensional Solution Structure of a DNA Duplex Containing the *Bcl*I Restriction Sequence: Two-Dimensional NMR Studies, Distance Geometry Calculations, and Refinement by Back-Calculation of the NOESY Spectrum†

Kevin M. Banks,‡ Dennis R. Hare,§ and Brian R. Reid*,‖

Departments of Chemistry and of Chemistry and Biochemistry, University of Washington, Seattle, Washington 98195, and Hare Research, Woodinville, Washington 98072

Received August 1, 1988; Revised Manuscript Received May 10, 1989

ABSTRACT: A three-dimensional solution structure for the self-complementary dodecanucleotide [d-(GCCTGATCAGGC)]$_2$ has been determined by distance geometry with further refinements being performed after back-calculation of the NOESY spectrum. This DNA dodecamer contains the hexamer [d(TGATCA)]$_2$ recognized and cut by the restriction endonuclease *Bcl*I, and its structure was determined in hopes of obtaining a better understanding of the sequence-specific interactions which occur between proteins and DNA. Preliminary examination of the structure indicates the structure is underwound with respect to idealized B-form DNA though some of the local structural parameters (glycosyl torsion angle and pseudorotation angle) suggest a B-family type of structure is present. This research demonstrates the requirements (resonance assignments, interproton distance measurements, distance geometry calculations, and NOESY spectra back-calculation) to generate experimentally self-consistent solution structures for short DNA sequences.

The recognition of short DNA sequences by proteins (operator sequences by repressors, promoter sequences by RNA polymerase, and restriction sequences by endonucleases) is remarkably specific (Ohlendorf & Matthews, 1983). The affinities between these DNA sequences and their specific proteins are known to be regulated by a number of highly sensitive intermolecular forces, which include electrostatic interactions between the positively charged amino acids and the negatively charged phosphate backbone, sequence-specific intermolecular hydrogen bonding, and van der Waals interactions (Berg & Blomberg, 1978; Berg et al., 1981; Takeda et al., 1986; von Hippple & McGhee, 1972; Ohlendorf & Matthews, 1983). These facts suggest that the three-dimensional structure of the DNA, as well as that of the protein, must play a tremendously important role in the protein/DNA recognition phenomenon (Lomonossoff et al., 1981; Rhodes, 1982; Drew & Travers, 1984, 1985). Within the recent literature, various DNA sequences have been studied with many different spectroscopic techniques with the aim of determining their three-dimensional structures: the goal of these studies was to obtain a better understanding of the mechanisms that regulate DNA-protein interactions (Dickerson & Drew, 1981; Shakked et al., 1983). Additionally, the application of two-dimensional ^{1}H nuclear magnetic resonance spectroscopy (NMR) methods to biopolymers has proven to be a powerful technique, yielding an abundance of structural information when used carefully. In particular, the observation and interpretation of the nuclear Overhauser effect (NOE), a dipolar,

†Supported in part by Program Project Grant P01GM 32681 to B.R.R. and SBIR Grant GM 35620 to D.R.H.
‡Department of Chemistry, University of Washington.
§Hare Research.
‖Department of Chemistry and Biochemistry, University of Washington.

0006-2960/89/0428-6996$01.50/0

through-space coupling between neighboring protons (up to 5.0 Å apart), is especially useful in yielding three-dimensional structural insights for small proteins (Bystrov, 1976; Bundi & Wüthrich, 1979; Kline & Wüthrich, 1986; Williamson et al., 1985; Weber et al., 1985, 1987) and short nucleic acid duplexes (Hare et al., 1983; Reid et al., 1983; Clore & Gronenborn, 1983; Scheek et al., 1983; Wemmer et al., 1984a; Lefèvre et al., 1987; Kintanar et al., 1987). These structural insights, useful as they are, are usually only rough estimates of local molecular structure since, at the longer mixing times necessary to observe most of the NOE's, spin diffusion occurs (Hull & Sykes, 1975; Kalk & Berendsen, 1976; Bothner-By & Noggle, 1979), making the NOE intensity only a rather qualitative estimate of distance.

A more rigorous approach to obtain quantitative distance information in biopolymers involves monitoring the time-dependent NOE buildup rate for each dipolar-coupled pair of protons (Hull & Sykes, 1975; Kumar et al., 1981; Noggle & Schirmer, 1971). At short mixing times, before higher order spin-diffusion processes become significant, the distance between protons of unknown separation can be estimated by scaling the initial NOE growth rate to the growth rate corresponding to a reference fixed distance with the equation[1]

$$R_{1(\mathrm{ref})}/R_{1(ij)} = r_{ij}^6/r_{\mathrm{ref}}^6$$

In DNA duplexes, either the cytosine H5–H6 distance (2.46 Å) or the geminal H2′–H2″ sugar distance (1.78 Å) can be used as a known fixed distance; the initial growth rate (15–20 ms) of these reference NOESY crosspeaks scale as the sixth power of distance, indicating that sugar protons and base protons have the same correlation time (Reid et al., submitted for publication). Structural arguments based on these interproton distances can then be made, yielding fairly accurate estimates of local geometries. Beginning with a sufficient number of such distances, one can, in theory, determine the structure of the molecule using distance geometry methods (Havel et al., 1979; Havel & Wüthrich, 1985). Recently, structures of a number of different DNA oligonucleotides have been determined with two-dimensional NMR and distance geometry techniques. These include the solution structure of a dodecamer hairpin (Hare & Reid, 1986), a duplex with a base pair mismatch (Hare et al., 1986a), a duplex with an extrahelical residue (Hare et al., 1986b), and a promoter sequence (Nerdal et al., 1988). However, one must be careful when analyzing these structures and other published DNA structures in detail. In generating a number of reasonably superimposable structures based on NOE distances, whether one uses distance geometry (which builds the structure from the distance constraints), least-squares refinement (Clore et al., 1985a,b), or restrained molecular dynamics [which uses energy potentials in addition to the NOE constraints—Nilges et al. (1987a,b)], one cannot necessarily conclude that the actual structure of the molecule (or even the family of structures within which the actual structure might exist) has been defined. Instead, by generating a family of superimposable structures, one has merely shown that the interproton distances (in the case of distance geometry) in addition to the energy potentials (in the case of restrained molecular dynamics) have been satisfied and that the appropriate computer algorithm to optimize these parameters is working correctly. This subtlety necessitates the need for a device other than molecular superimpositions with which to assess structural accuracy. Probably the most rigorous test of structural accuracy is back-calculation of the NOESY spectrum corresponding to the proton coordinates of the determined structure at all mixing times. If the back-calculated NOESY spectra and the experimental spectra match well, one can conclude that the structure not only satisfies the proton–proton distance constraints but is also consistent with the entire proton relaxation network that generates the time-dependent NOESY spectra. This latter criterion is much more rigorous and difficult to satisfy than simple distance agreement.

In this paper we describe the processes (assignments, distance geometry calculations, and NOESY back-calculations followed by iterative refinement) which were used to determine the structure of the symmetrical DNA dodecamer [d-(GCCTGATCAGGC)]$_2$ containing the *Bcl*I restriction sequence. The final refined structure satisfies the experimental NOESY data very well at six mixing times. The central hexamer of the DNA dodecanucleotide [d(TGATCA)]$_2$ is the sequence that is bound and cleaved by a type II restriction endonuclease found in *Bacillus caldolyticus* (Bingham et al., 1978). For the NMR studies, we added three base pairs, [d(GCC···GGC)]$_2$, to both ends of the *Bcl*I restriction sequence to buffer the biologically active hexanucleotide from end-fraying effects. The restriction endonuclease *Bcl*I is active as a dimer with a molecular mass of 25 000 daltons per subunit and belongs to the same family of restriction recognition endonucleases as *Bam*HI, *Bgl*II, and *Mbo*I since all four enzymes have the same internal recognition sequence [d(GATC)]$_2$. Furthermore, in all four cases, the site of cleavage is identical, [d(N↓GATCN)]$_2$, with GATC sticky ends being generated. By determining and analyzing the structure of the *Bcl*I restriction sequence and other related restriction sequences, we hope to gain insights into how the sequence, structure, and function are related and to elucidate the mechanisms by which restriction endonucleases recognize and cleave their specific restriction sites.

Materials and Methods

Sample Preparations. The DNA dodecanucleotide [d-(GCCTGATCAGGC)]$_2$ containing the *Bcl*I restriction sequence was synthesized on an Applied Biosystems 380A DNA synthesizer on a 10-μmol scale according to solid-phase phosphite triester techniques described previously (Hare & Reid, 1986). The synthetic DNA sample was purified by chromatography on Sephadex G-25 columns 120 cm in length. Each fraction was checked for purity by analytical gel electrophoresis and pooled accordingly. Approximately 40 mg of purified material was lyophilized to dryness and dissolved in 0.4 mL of 20 mM sodium phosphate buffer, pH 7.0, containing 50 mM NaCl. The sample was repeatedly lyophilized to dryness from 99.96% D_2O, dissolved in 0.4 mL of 99.995% D_2O, and transferred to a NMR tube. For spectroscopy in H_2O, the final solution contained 20 mM sodium phosphate, pH 7.0, 50 mM NaCl, and 10% D_2O in a volume of 0.4 mL.

NMR Spectroscopy. ^{1}H NMR experiments were carried out on a Bruker WM-500 spectrometer at a sample temperature of 37 °C. Six NOESY spectra with mixing times of 30, 60, 90, 120, 150, and 180 ms were acquired consecutively in an arbitrary order during a single 5-day period without the sample being removed from the probe. These pure absorption NOESY spectra (Macura & Ernst, 1980) were collected by phase-sensitive methods (States et al., 1982). The NOESY data were collected into 1024 complex points in t_2 and 400 points in t_1 with 32 scans per t_1 experiment, a relaxation delay of 2 s between scans being used. The residual HDO signal was not suppressed in any of the spectra due to its relatively low intensity, and for each experiment, the carrier frequency

[1] This equation is valid only when the two pairs of protons have the same correlation time τ_c and the product $\omega\tau_c$ is much greater than 1.

was placed in the center of the spectrum (Rance et al., 1983).

Exchangeable proton spectra were obtained in 90% H_2O with a Redfield 214 pulse of about 280 μs tailored to null at the H_2O frequency by placing with the carrier frequency at 11.5 ppm (Redfield, 1978). The H_2O NOESY spectrum was collected as a magnitude spectrum into 1024 complex points in t_2 and 280 points in t_1 with 138 scans per experiment and a mixing time of 300 ms.

Following collection, the acquired data were copied onto magnetic tape and transferred to a MICRO VAX II for processing with FTNMR software (Hare Research Inc.). The NOESY data sets were zero filled to 2048 points in t_2 and multiplied by a window function with a value of 1.0 for the first 1248 points which then smoothly dropped to 0 at 2048 points as a sine bell squared function in order to minimize truncation effects without affecting crosspeak volumes. After Fourier transformation, the data were also phase corrected to yield pure absorptive line shapes. In the t_1 dimension, the NOESY data were zero filled to 2048 complex points (Bartholdi & Ernst, 1973) and multiplied by a window function which had a value of 1.0 for the first 280 points and then decreased smoothly as a sine bell squared window function to 0 at 400 points to minimize truncation effects on protons with longer T_2. Fourier transformation and phase correction completed the data processing. In all spectra, t_1 ridge noise was attenuated by multiplying the first row after the t_2 transform by one-half (Otting et al., 1986). The NOESY spectrum of the nonexchangeable protons was processed as described above, except that a shifted sine bell function was applied to the data in both the t_2 and the t_1 dimensions.

Determining Distance Constraints. To convert NOE buildup rates into distances, the two-spin approximation was used at short mixing times (Noggle & Schirmer, 1971; Kalk & Berendsen, 1976; Wagner & Wüthrich, 1979). Starting distances between pairs of protons were determined by scaling the initial NOE buildup rate of the corresponding crosspeak to the initial NOE buildup rate found for the cytosine H5–H6 crosspeaks which correspond to a distance of 2.46 Å. Since we have shown that there is no significant nanosecond local motion for the sugar moieties in DNA (Reid et al., submitted for publication), all distances except those involving methyl groups can be calculated using the H5–H6 correlation time. For all NOE's to methyl groups, a thymine H6–M5 pseudo atom distance of 2.9 Å was used as the reference distance (Tropp & Redfield, 1981)—methyl protons have different relaxation characteristics than non-methyl protons and must be treated as separate entities (Kalk & Berendsen, 1976). We ignored the C3 axis angle dependence of methyl cross-relaxation, leading to some inaccuracy in our methyl distance estimates. For determining distances from crosspeaks between exchangeable protons, we used a qualitative weak (3.5–5.0 Å), medium (2.5–3.5 Å), and strong (2.0–2.5 Å) approach similar to that used for determining interproton distances in proteins (Havel & Wüthrich, 1984).

Distance Geometry Calculations. The concepts and details of distance geometry have been described extensively in the literature (Havel et al., 1983a,b; Crippen, 1977) and will not be discussed in detail here. All of the distance geometry calculations were performed on a Convex C1 computer using the DSPACE program (D. R. Hare and R. D. Morrison, unpublished data). A more detailed description of the subroutines and macros (which are defined by the user) within DSPACE has been presented elsewhere (Hare & Reid, 1986; Hare et al., 1986a,b; Nerdal et al., 1988), and only a brief description of the application of DSPACE to the present problem will appear here. To initiate the distance geometry calculation, upper and lower bounds were assembled for all distances implicit in the primary structure and stored in a bounds matrix, with the experimentally determined interproton distance bounds being added last. In addition, interbase cross-strand NH···N and NH···O distances were entered into the distance matrix as standard H-bond lengths, on the basis of the observation of a downfield-shifted H-bonded resonance for each of these protons. The bounds matrix was then subjected to several smoothing techniques to improve the bounds (Nerdal et al., 1988). At this stage, several different distance matrices were generated by choosing random numbers between the upper and lower bounds for each matrix element—producing several symmetrical trial matrices, each of which was embedded in 3-space via conversion to a metric matrix and evaluation of the three largest eigenvalues. The initially embedded coordinates for each structure were then refined by a combination of conjugate gradient refinement and a simulated annealing algorithm, which uses deviations from the distance bounds as a penalty. When the penalty function of the current structure became sufficiently small, a symmetry penalty was applied (the two DNA strands are known to be symmetrical from the NMR spectrum), and further conjugate gradient refinement was performed, increasing the molecular symmetry. This process was carried out eight times, starting with a different randomly embedded structure each time, leading to eight independent structures whose pairwise root-mean-squared deviations (RMSD) were fairly small (typically 1.2–2.2 Å).

Back-Calculation of NOESY Spectra from Structures. The NOESY spectrum of a discrete structure can be calculated by numerical integration of the Bloch equations. In the slow motion limit, the cross-relaxation process dominates—thus the most important consideration for correctly simulating the spectrum is spin diffusion. We begin by determining, as accurately as possible, two relaxation rate parameters that describe the spectral density empirically. The first quantity is a cross-relaxation scaling parameter that, when combined with the actual proton–proton distance separation, gives the NOE cross-relaxation rate. We assume that the cross-relaxation scaling parameter is constant throughout the molecule. The second parameter is "Z leakage" which includes all other processes by which a spin loses Z magnetization during the NOESY mixing time. This value includes all longitudinal relaxation processes other than the zero-quantum "spin flip", as well as solvent exchange. Z leakage is calculated by measuring the time course of measurable autopeaks in the spectrum and subtracting their respective cross-relaxation components; this parameter is closely approximated by measuring the decay rate of the total of all points in a NOESY spectrum as a function of mixing time. The only spins we have observed that deviate significantly from this general overall lattice-leakage rate are those involved in chemical exchange with solvent.

Simulating the NOESY is quite straightforward once one has calculated the relative cross-relaxation scaling factor and Z leakage components for each assigned proton. First, for each pair of protons within some predetermined cutoff distance (typically 5 Å), a list is generated which contains all protons within the cutoff radius to either proton in the pair. The initial Z magnetizations are set up as in the NOESY experiment, and the evolution of Z magnetization throughout the whole molecule is calculated numerically and examined at times corresponding to the experimental mixing times. Using a time increment of 1 ms yields crosspeak intensity buildups that are indistinguishable from those generated by diagonalizing the

Table I: Assignments of the DNA Duplex Containing the *Bcl*I Restriction Sequence

1 12
5′-G-C-C-T-G-A-T-C-A-G-G-C-3′
3′-C-G-G-A-C-T-A-G-T-C-C-G-5′
12 1

residue	H8	H6	H5	H2	CH_3	H1′	H2″	H2′	H3′	H4′
G1	7.91					5.93	2.72	2.61	4.79	4.10
C2		7.51	5.36			6.06	2.50	2.22	4.84	4.25
C3		7.53	5.56			5.93	2.46	2.06	4.79	4.10
T4		7.27			1.62	5.67	2.38	2.00	4.84	4.20
G5	7.88					5.59	2.78	2.69	4.99	4.34
A6	7.18			7.67		6.19	2.88	2.58	4.95	4.43
T7		7.09			1.30	5.83	2.39	1.96	4.80	4.12
C8		7.44	5.57			5.46	2.29	1.94	4.79	4.06
A9	8.12			7.53		5.90	2.82	2.66	4.99	4.34
G10	7.59					5.52	2.61	2.50	4.93	4.31
G11	7.62					5.92	2.65	2.44	4.89	4.34
C12		7.33	5.21			6.10	2.20	2.16	4.46	3.99

rate matrix (P. Mirau, personal communication). For large molecules, it would seem that this numerical approach should be considerably faster than the analogous rate matrix approach.

In addition to its use in evaluating the accuracy of structures, back-calculation can be used for the further refinement of these structures in order to obtain consistency with experimental NOESY data. Since distances estimated directly from NOE data (the forward calculation) are prone to errors, back-calculation of NOESY spectra from structures provides the user with a means of adjusting those structures to better agree with the experimental data. One identifies simulated crosspeaks that are too big or too small compared to their experimental intensities at any mixing time; the corresponding distance bounds are then adjusted in the proper direction. Another advantage of the back-calculation lies in the fact that all spins, not only those that have been assigned and measured, are considered in the NOESY simulation.

Agreement with experimental NOESY data is an essential requirement for NMR-based structure determination, but because one can reproduce experimental data, one cannot assume that an accurate structure has been determined. We believe, however, that the method is a major improvement over previous qualitative or semiquantitative structural work based on NMR data.

Results and Discussion

NMR Assignments. The resonance assignments for the *Bcl*I DNA duplex (Table I) were made by use of assignment strategies for B-like DNA developed earlier by several investigators (Feigon et al., 1982; Clore & Gronenborn, 1983; Hare et al., 1983; Reid et al., 1983; Scheek et al., 1983; Wemmer et al., 1984a,b). The basis of the assignment strategy is the sequential connection of the base and sugar protons with NOE's. There are several pathways by which a proton on a particular residue can cross-relax via protons on adjacent residues; these pathways have been well-defined in right-handed B-like DNA, and misassignments, especially in a duplex containing only 12 unique nucleotides, are extremely unlikely. Nevertheless, as an additional safeguard, a phase-sensitive double quantum filtered COSY spectrum (Aue et al., 1976; Rance et al., 1983) was acquired to confirm the assignment of scalar coupled protons.

The one-dimensional spectrum of the nonexchangeable protons of the *Bcl*I dodecamer $[d(GCCTGATCAGGC)]_2$ is shown in Figure 1. The proton resonances are grouped into relatively distinct regions and are fairly well resolved within each spectral region. The sample temperature was adjusted

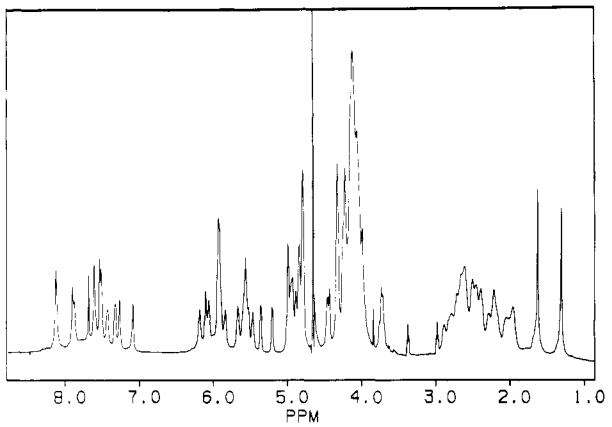

FIGURE 1: One-dimensional 500-MHz ^1H NMR spectrum of the DNA dodecamer $[d(GCCTGATCAGGC)]_2$ containing the *Bcl*I restriction site in D_2O. The spectrum was accumulated into 8192 data points with 32 scans and a spectral width of 4386 Hz. The temperature of the sample was 37 °C. Apodization with a shifted sine bell has been applied to the one-dimensional spectrum to enhance resolution.

to minimize overlap of the residual HDO with any of the DNA protons, making assignments for the H3′ and H4′ resonances easier to define. The chemical shifts of the four cytosine H5 and H6 resonances as well as the two thymine methyl and H6 resonances were identified from the DQF-COSY spectrum and represent excellent starting points for the sequential assignment procedure. Figure 2 shows the region of the 180 ms mixing time NOESY spectrum which includes the base to 2′H/2″H and methyl proton crosspeaks—the latter appear on the right side of the figure. Each of the two thymine methyl resonances shows crosspeaks to two base protons (connected by a vertical line); the upfield (7.15 and 7.30 ppm) pair of crosspeaks are intraresidue NOE's from thymine methyl to their own H6, confirmed in the COSY spectrum, while the downfield pair of crosspeaks correspond to thymine methyl to 5′ adjacent base proton NOE's. From the sequence, the two bases on the 5′ side of the two thymines (T7 and T4) are an adenine and a cytosine at positions 6 and 3, respectively. The base protons of the four cytosine residues (C2, C3, C8, and C12) are easily identified in the DQF-COSY spectrum and in the NOESY base to H1′ region (Figure 3) as very strong H5–H6 crosspeaks. The resonance at 7.56 ppm is therefore the H6 of C3, and the resonance at 8.13 ppm is the H8 of A6.

With the C3, T4, A6, and T7 base proton chemical shifts in hand, we next turned to the NOESY region containing crosspeaks between base protons and sugar H1′ resonances (left portion of Figure 3). As established earlier, for right-

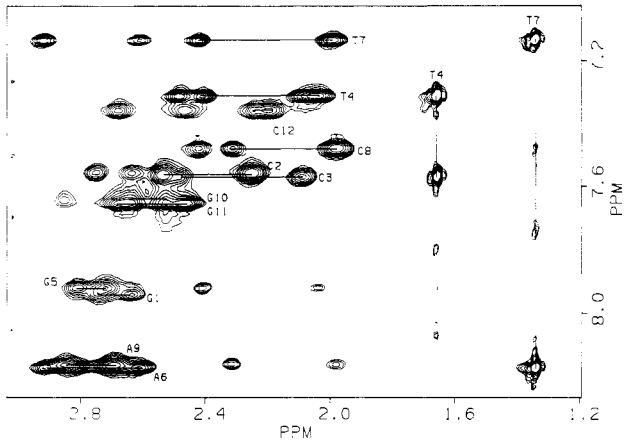

FIGURE 2: Expansion of the NOESY spectrum of the *BclI* restriction site showing the base to H2′R, H2′S, and methyl resonance crosspeak region. The crosspeaks between base and the H2′R (downfield) and H2′S (upfield) resonances of the same residue have been labeled with the residue number and connected with a horizontal line. The base to methyl NOE's have been labeled with the identity of the thymine residue on which the methyl resides and are indicated by vertical bars. Those crosspeaks which are not labeled represent long-range NOE's from a base proton to the H2′R and H2′S resonances of the residue directly to the 5′ side.

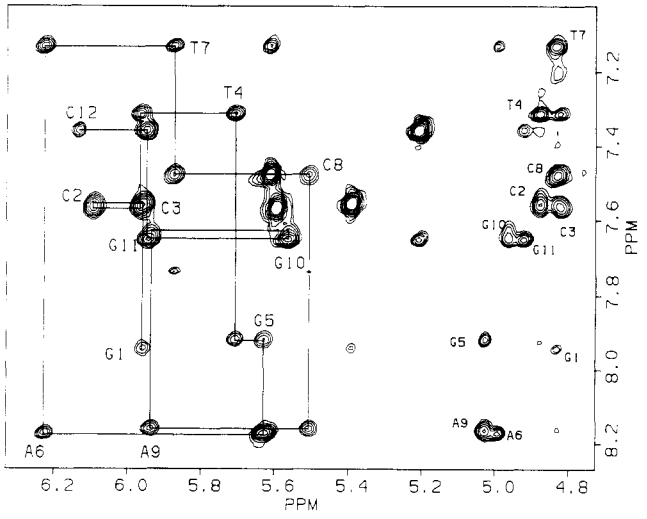

FIGURE 3: Expansion of the NOESY spectrum of *BclI* showing the base H8/H6 to sugar H1′ crosspeaks. The sequential connectivity walk has been traced for each of the strands starting at either end of the helix. The crosspeaks between the base protons and H1′ resonances of the same residue have been labeled with that residue's number. The four intense crosspeaks in the center of the spectrum represent cytosine H6–H5 NOE's and are not labeled though their assignments can be determined unambiguously be observing the residue label of crosspeaks with the same base proton chemical shift. The right portion of the spectrum shows crosspeaks between base protons and their own H3′ resonances and are labeled as such.

handed B-like DNA, NOE's occur between the base proton of a particular residue and the H1′ resonance of the preceding (5′) residue as well as to its own sugar H1′ and vice versa. Starting from the base proton of T7 and proceeding toward the H8 of A6 (8.13 ppm) in the 5′ direction, one can perform a sequential walk, making connectivities between the base and H1′ protons for residues T7 to C3. The connectivity from the base proton of C3 to the H1′ proton of C2 is complicated by overlapping crosspeaks, but one is able to get through this portion of the sequence without much difficulty since the H6 protons of C3 and the other three cytosine residues are known from their intense COSY and NOESY H5–H6 crosspeaks. To complete the base assignments to the 5′ end of the helix, the connectivity from the H1′ of C2 to the H8 of G1 was made,

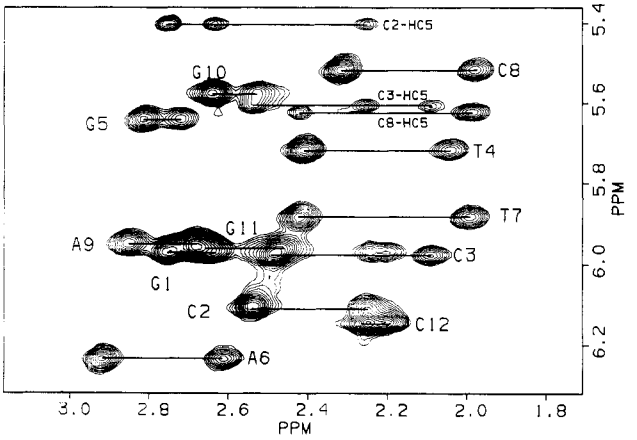

FIGURE 4: Expansion of the NOESY spectrum of *BclI* showing the H1′ to H2′R and H2′S crosspeaks. The H2′R and H2′S crosspeaks of each sugar have been connected and labeled with a horizontal line for the residue from which they arose. In addition weak NOE's between the cytosine H5 resonance and the H2′ of nearby sugars are observed and are labeled with the smaller text.

aided by the presence of a NOE between the base proton of G1 and the H5 resonance of C2. As expected, G1 H8 has only one H1′ NOE (its own anomeric proton). The base and H1′ resonances for the 3′ half of the helix were identified by starting at T7 and stepping along the chain in the opposite direction. The crosspeaks of the walk are well-resolved connecting residues T7, C8, and A9, but similar chemical shifts of the H8 resonances of G10 and G11 make complete assignments for this end of the helix more difficult. Careful observation shows, however, that the only possible pathway from the remaining cytosine base proton (C12) to the base proton of A9 is the one shown in Figure 3.

Partial assignments for the deoxyribose H2′R and H2′S (according to IUPAC nomenclature, H2′R and H2′S correspond to the 2″ and 2′ protons, respectively) resonances as well as confirmation of the previous base assignments were made with the expansion of the NOESY spectrum shown in Figure 2. For each residue in B-type DNA, NOE's are expected to occur from a base resonance to both the H2′R and H2′S of its own deoxyribose with the NOE to its own H2′S resonance (usually upfield) being stronger than to the H2′R; this pattern can vary, however, depending on the exact sugar conformation. These intranucleotide NOE's, though many are not well resolved, are connected by a horizontal line in Figure 2. Because of the relatively long 180-ms mixing time, this particular NOESY spectrum also shows crosspeaks between the base resonances and the H2′R and H2′S resonances of the neighboring 5′-sugar. By vertically connecting these interresidue NOE's to the known intraresidue NOE's of the preceding neighbor, one can perform a base–H2′ sequential walk (not shown) that establishes an independent means by which one can assign base and sugar resonances. To definitively assign the deoxyribose 2′-protons, one must examine the NOESY H1′–H2′R/H2′S crosspeak region shown in Figure 4 armed with the H1′ assignments from Figure 3. For all but one of the H1′ resonances, only intraresidue NOE's from the H1′ to the weaker H2′S (upfield) and stronger H2′R (downfield) are observed (the H2′S can never be closer than the H2′R to the H1′ in D-deoxyribose). The self-consistence of the base–H1′, base–H2′/H2″, and H1′–H2′/H2″ connectivities, together with the COSY spectrum, leads to unambiguous and definitive assignments for these protons in each residue.

Assignment of the H3′ and H4′ resonances was made by examining the NOESY spectrum in two separate regions. Crosspeaks from the bases to their own H3′ (the right portion

of Figure 3), though fairly weak, are seen to be stronger than base NOE's to the 5′-adjacent H3′, allowing moderately confident assignments for the H3′ resonances to be made. These assignments can be confirmed by examination of the NOESY H1′ to H3′ crosspeak region where intraresidue crosspeaks are apparent for most of the residues, and also from the H2′/H2″ to H3′ NOESY and COSY spectra. The H4′ chemical shifts were identified from the expected intraresidue H1′–H4′ crosspeaks, which are stronger and sharper than the interresidue H1′–H5′ crosspeaks also found in this region. In the few cases where the H1′–H4′ crosspeaks were not readily distinguishable due to overlaps, the COSY of the H3′–H4′ region and the NOESY of the H2′–H4′ region (data not shown) were examined to yield consistent assignments. Assignments for the H5′ and H5″ resonances for the *BclI* sequence were not attempted due to the poor spectral resolution in the region between 4.0 and 4.4 ppm. In theory, one can assign the H5′ resonances via H4′–H5′ COSY crosspeaks and H1′ to (n + 1) H5′ NOESY crosspeaks, although in practice even DQF-COSY spectra do not yield the spectral resolution necessary to make *stereospecific* assignments (except for the chemically shift redundant upfield-shifted H5′ resonance of G1). Assignments for the imino resonances (data not shown since the chemical shifts of the imino protons are temperature and salt dependent) were made with a magnitude NOESY following techniques described previously (Chou et al., 1983).

From the described assignment protocol, resonance assignments for all the nonexchangeable protons except the H5′ and H5″ were made (84 proton assignments in all). In addition, assignments were made for five of the six imino protons. Thus, with complete assignments in hand and each crosspeak being identified by its cross-relaxing protons, distances for each well-resolved crosspeak were next determined.

Distance Measurements and Qualitative Structural Interpretation. Following the assignment of the *BclI* dodecamer spectrum, interproton distances were calculated for each of the resolved crosspeaks by measuring their initial rate of cross-relaxation. This was carried out by plotting the measured volume intensities as a function of mixing time from 30 to 180 ms for all nonoverlapped crosspeaks found within the NOESY spectra, as described under Materials and Methods. An initial qualitative evaluation of the structure was then made. In the overall sense, the distances determined for the dodecamer containing the *BclI* recognition sequence are consistent with those of the broad family of B-like DNA in that, qualitatively, the intranucleotide and internucleotide distance ranges characteristic of B-like DNA are observed. This fact is important in itself as it adds to our confidence in the biological relevance of the work in that these short synthetic pieces of DNA exhibit many of the features previously suggested for longer DNA segments. However, one must be careful because the DNA dodecamer containing the *BclI* restriction sequence, unlike classical B-form DNA, appears not to be absolutely regular in structure in that wide differences in the distances between the same types of protons within different residues can be found. In particular, the presence of an unusually short distance, 2.6 Å, for the interresidue H8(6)–H1′(5) crosspeak (Figures 3 and 5), is markedly different from the distance expected for this type of connectivity in regular B-form DNA. Conversely, a rather large distance of ca. 3.95 Å (see Table II) was found between the analogous H8 of G5 and the sugar H1′ of T4. The presence of variation in the base to H1′ distances can be seen even more clearly in Figure 6 where the NOE buildup rates for several representative crosspeaks are plotted. Again, it is obvious from these data that the distances

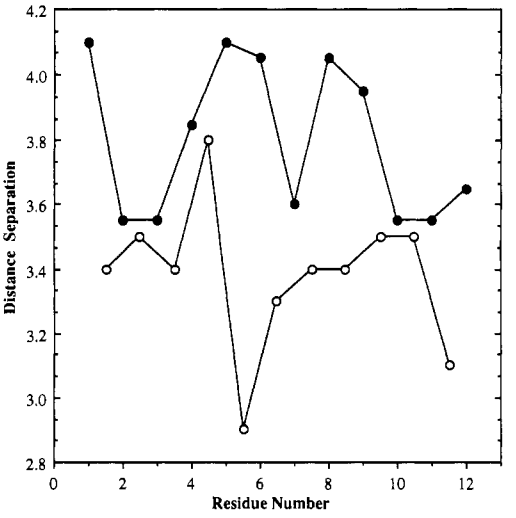

FIGURE 5: Graph showing the distance separation as a function of residue number for base to H1′(n − 1) (open circles) and the base to H1′(n) (solid circles) crosspeaks. Although the overall average distances compare well to those found for idealized B-form DNA, distances at a local level can deviate by large amounts. In particular, the base–H1′(n − 1) distance for the G5-T4 step is very large (3.8 Å) whereas the following base–H1′(n − 1) distance for the A6-G5 step is quite short (2.9 Å).

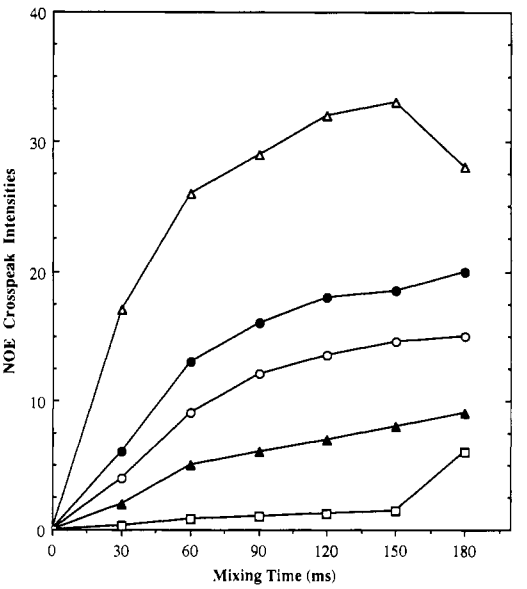

FIGURE 6: NOE buildup rates for the H6(7)–H2′S(6) (open diamonds, 2.4 Å), H8(6)–H1′(5) (solid circles, 2.9 Å), H8(6)–H2′R(6) (open circles, 3.0 Å), H6(7)–H1′(6) (solid triangles, 3.3 Å), and H8(6)–H1′(6) (open squares, 4.1 Å) crosspeaks. This plot shows the type of data used to calculate starting distances from the initial NOE buildup rates.

between similar proton types on different residues vary significantly. Thus, while the overall average structure of the dodecamer we are studying is B-like, there appears to be a large amount of local structural variation present, not unlike that observed by Dickerson and Drew (1981) for the crystal structure of a B-DNA dodecamer.

A somewhat complementary variation in the distance from the base H6/H8 to its own sugar H1′ was observed in the *BclI* dodecamer. For idealized B-form DNA, this distance is 3.78 Å, yet our measured distances indicate that, while the *average* base–H1′(own) distance is approximately 3.8 Å, only in the case of T4 was this distance actually found to be 3.8 Å. For each of the other residues, the base–H1′(own) distances varied from 3.5 to 4.1 Å (Figure 5). Similar variations were also

Table II: Distance Constraints for the Symmetrical *BclI* Restriction Dodecamer Derived from NOE Buildup Rate Measurements

atom pair	lower bound (Å)	upper bound (Å)	atom pair	lower bound (Å)	upper bound (Å)	atom pair	lower bound (Å)	upper bound (Å)	atom pair	lower bound (Å)	upper bound (Å)
Base Proton to Base Proton Constraints						**h1′ to h3′ Constraints**					
h8[1]-h8[2]	3.6	5.0	h6[3]-h6[4]	4.0	4.7	h1′[2]-h3′[2]	3.7	4.2	h1′[4]-h3′[4]	3.4	4.0
h6[4]-h8[5]	3.8	4.7	h8[5]-h8[6]	4.0	4.7	h1′[5]-h3′[5]	3.5	4.0	h1′[6]-h3′[6]	3.7	4.2
h8[6]-h6[7]	3.8	4.7	h6[7]-h6[8]	4.0	4.7	h1′[7]-h3′[7]	3.5	4.1	h1′[8]-h3′[8]	3.6	4.2
h6[8]-h8[9]	4.2	4.7	h8[9]-h8[10]	4.2	4.7	h1′[9]-h3′[9]	3.6	4.4	h1′[10]-h3′[10]	3.5	4.0
h8[11]-h6[12]	4.2	5.0				h1′[11]-h3′[11]	3.8	4.4	h1′[12]-h3′[12]	3.5	4.2
h1′ to Base Proton Constraints						**h1′ to h4′ Constraints**					
h1′[1]-h8[1]	3.9	4.3	h1′[1]-h6[2]	3.2	3.6	h1′[2]-h4′[2]	3.0	3.4	h1′[4]-h4′[4]	2.8	3.2
h1′[2]-h6[2]	3.2	3.9	h1′[2]-h6[3]	3.3	3.7	h1′[5]-h4′[5]	2.8	3.2	h1′[6]-h4′[6]	3.0	3.4
h1′[3]-h6[3]	3.2	3.9	h1′[3]-h6[4]	3.3	3.7	h1′[7]-h4′[7]	2.9	3.5	h1′[8]-h4′[8]	2.8	3.2
h1′[4]-h6[4]	3.7	4.0	h1′[4]-h8[5]	3.8	4.1	h1′[10]-h4′[10]	2.8	3.2	h1′[12]-h4′[12]	2.8	3.8
h1′[5]-h8[5]	3.9	4.3	h1′[5]-h8[6]	2.5	2.7						
h1′[6]-h8[6]	3.9	4.2	h1′[6]-h6[7]	3.4	3.7	**h1′ to h2′R Constraints**					
h1′[7]-h6[7]	3.4	3.8	h1′[7]-h6[8]	3.3	3.7	h1′[1]-h2′R[1]	2.8	3.3	h1′[2]-h2′R[2]	2.8	3.4
h1′[8]-h6[8]	3.7	4.4	h1′[8]-h8[9]	3.3	3.7	h1′[3]-h2′R[3]	2.9	3.3	h1′[4]-h2′R[4]	2.8	3.2
h1′[9]-h8[9]	3.8	4.1	h1′[9]-h8[10]	3.3	3.7	h1′[5]-h2′R[5]	2.8	3.1	h1′[6]-h2′R[6]	2.8	3.1
h1′[10]-h8[10]	3.2	3.9	h1′[10]-h1′[11]	3.3	3.7	h1′[7]-h2′R[7]	2.7	3.1	h1′[8]-h2′R[8]	2.8	3.2
h1′[11]-h8[11]	3.2	3.9	h1′[11]-h6[12]	2.9	3.3	h1′r10]-h2′R[10]	2.8	3.2	h1′[12]-h2′R[12]	2.7	3.2
h1′[12]-h6[12]	3.3	4.0	h1′[6]-h2[6]	4.0	5.0						
h1′[7]-h2[6]	3.9	4.8	h1′[20]-h2[6]	4.3	5.0	**h1′ to h2′S Constraints**					
						h1′[1]-h2′S[1]	2.3	2.5	h1′[2]-h2′S[2]	2.2	2.4
h5 to Base Proton Constraints						h1′[4]-h2′S[4]	2.2	2.4	h1′[5]-h2′S[5]	2.3	2.4
h5[2]-h8[1]	4.2	5.0	h5[8]-h6[7]	3.3	3.9	h1′[6]-h2′S[6]	2.2	2.5	h1′[7]-h2′S[7]	2.2	2.5
h5[12]-h8[11]	3.3	3.9				h1′[8]-h2′S[8]	2.2	2.4	h1′[9]-h2′S[9]	2.3	2.5
						h1′[10]-h2′S[10]	2.4	2.7	h1′[12]-h2′S[12]	2.2	2.4
h3′ to Base Proton Constraints											
h3′[1]-h8[1]	4.5	4.9	h3′[2]-h6[2]	3.9	4.3	**h5 to h2′R and h2′S Constraints**					
h3′[3]-h6[3]	3.8	4.2	h3′[3]-h6[4]	4.3	4.6	h5[2]-h2′R[1]	3.3	3.8	h5[2]-h2′S[1]	3.0	3.3
h3′[4]-h6[4]	4.4	4.8	h3′[4]-h8[5]	4.4	5.0	h5[2]-h2′R[2]	3.3	3.9	h5[2]-h2′S[2]	3.6	4.0
h3′[5]-h8[5]	4.3	4.7	h3′[6]-h8[6]	4.4	4.8	h5[3]-h2′R[2]	3.3	4.0	h5[3]-h2′S[3]	3.8	4.3
h3′[6]-h6[7]	4.6	5.0	h3′[7]-h6[7]	4.2	4.5	h5[3]-h2′R[3]	3.3	4.0	h5[8]-h2′R[7]	3.2	3.7
h3′[8]-h6[8]	3.8	4.1				h5[8]-h2′S[7]	3.3	3.9	h5[12]-h2′S[11]	3.2	4.2
h3′[8]-h8[9]	4.4	4.7	h3′[9]-h8[9]	4.1	4.5	h5[12]-h2′R[12]	3.4	4.0			
h3′[9]-h8[10]	4.5	5.0	h3′[10]-h8[10]	4.1	4.5						
h3′[11]-h8[11]	4.3	4.8	h3′[11]-h6[12]	4.4	5.0	**h3′ to h2′R and h2′S Constraints**					
h3′[12]-h6[12]	4.3	4.7				h3′[1]-h2′R[1]	2.3	2.7	h3′[1]-h2′S[1]	2.6	3.1
						h3′[2]-h2′R[2]	2.5	2.8	h3′[2]-h2′S[2]	2.6	3.1
h2′R to Base Proton Constraints						h3′[3]-h2′S[3]	2.6	3.1	h3′[6]-h2′S[6]	2.7	3.2
h2′R[1]-h8[1]	2.2	2.6	h2′R[1]-h6[2]	2.7	3.6	h3′[8]-h2′S[8]	2.6	3.1	h3′[11]-h2′S[11]	2.5	3.2
h2′R[2]-h6[2]	2.2	2.5	h2′R[3]-h6[3]	2.2	2.4						
h2′R[3]-h6[4]	2.9	3.6	h2′R[4]-h6[4]	2.2	2.4	**Methyl Proton Constraints**					
h2′R[4]-h8[5]	3.3	4.1	h2′R[6]-h8[6]	2.2	2.6	m5[4]-h5[3]	3.3	4.3	m5[4]-h6[3]	2.9	3.7
h2′R[6]-h6[7]	3.0	3.4	h2′R[7]-h6[7]	2.3	2.4	m5[7]-h8[6]	2.7	3.3	m5[7]-h5[8]	3.6	4.6
h2′R[8]-h8[9]	3.3	4.0	h2′R[11]-h8[11]	2.3	2.8	m5[4]-h1′[3]	3.7	4.7	m5[4]-h3′[3]	3.7	4.7
h2′R[11]-h6[12]	2.9	3.6	h2′R[12]-h6[12]	2.3	2.6	m5[4]-h2′S[3]	3.3	4.3	m5[7]-h1′[6]	3.7	4.7
						m5[7]-h3′[6]	3.7	4.7	m5[7]-h2′R[6]	3.3	4.3
h2′S to Base Proton Constraints						m5[7]-h2′S[6]	3.3	4.3			
h2′S[1]-h8[1]	3.1	3.6	h2′S[1]-h6[2]	3.1	3.6						
h2′S[2]-h6[2]	2.9	3.3	h2′S[3]-h6[3]	3.0	3.6	**Constraints Involving Exchangeable Protons**					
h2′S[3]-h6[4]	2.5	2.9	h2′S[4]-h6[4]	2.8	3.2	h2[6]-hn3[19]	2.7	3.3	h2[9]-hn3[16]	2.7	3.3
h2′S[4]-h8[5]	3.2	3.9	h2′S[5]-h8[5]	2.8	3.3	h2[18]-hn3[7]	2.7	3.3	h2[21]-hn3[4]	2.7	3.3
h2′S[6]-h8[6]	3.0	3.4	h2′S[6]-h6[7]	2.7	3.2						
h2′S[7]-h6[7]	3.0	3.4	h2′S[7]-h6[8]	2.4	2.7	**Constraints from Assumed Interstrand Hydrogen Bonds**					
h2′S[8]-h6[8]	2.9	3.3	h2′S[8]-h8[9]	3.4	4.1	h1[1]-h1[23]	3.6	6.0	h1[23]-h1[22]	3.6	5.0
h2′S[9]-h8[9]	2.9	3.3	h2′S[9]-h8[10]	2.9	3.4	h1[22]-h3[4]	3.6	4.6	h3[4]-h1[5]	3.6	4.6
h2′S[10]-h8[10]	3.0	3.3	h2′S[11]-h8[11]	2.9	3.3	h1[5]-h3[19]	3.6	4.6	h3[19]-h3[7]	3.6	4.6
h2′S[11]-h6[12]	2.4	2.7	h2′S[12]-h6[12]	3.2	3.5	h3[7]-h1[17]	3.6	4.6	h1[17]-h3[16]	3.6	4.6
						h3[16]-h1[10]	3.6	4.6	h1[10]-h1[11]	3.6	5.0
						h1[11]-h1[13]	3.6	6.0			

Assumed Hydrogen Bonds (Å)

o6[1]-h4a[24]	1.86	h1[1]-n3[24]	1.849	h2a[1]-o2[24]	1.86
h4a[2]-o6[23]	1.86	n3[2]-h1[23]	1.849	o2[2]-h2a[23]	1.86
h4a[3]-o6[22]	1.86	n3[3]-h1[22]	1.849	o2[3]-h2a[22]	1.86
h3[4]-n1[21]	1.882	o4[4]-h6a[21]	1.964		
o6[5]-h4a[20]	1.86	h1[5]-n3[20]	1.849	h2a[5]-o2[20]	1.86
n1[6]-h3[19]	1.882	h6a[6]-o4[19]	1.964		
h3[7]-n1[18]	1.882	o4[7]-h6a[18]	1.964		
h4a[8]-o6[17]	1.86	n3[8]-h1[17]	1.849	o2[8]-h2a[17]	1.86
n1[9]-h3[16]	1.882	h6a[9]-o4[16]	1.964		
o6[10]-h4a[15]	1.86	h1[10]-n3[15]	1.849	h2a[10]-o2[15]	1.86
o6[11]-h4a[14]	1.86	h1[11]-n3[14]	1.849	h2a[11]-o2[14]	1.86
h4a[12]-o6[13]	1.86	n3[12]-h1[13]	1.849	o2[12]-2a[13]	1.86

apparent for the measured base proton to sugar H2′R/H2′S(n − 1) distances. For some of the base pair steps (A9-T8, G5-T4, G10-A9), these distances are much greater than in other base pair steps (T4-C3, C12-G11, C8-T7, C2-G1). The presence of variation in the base proton to sugar H2′R/H2′S(n − 1) distances suggests that some base pair steps may be either underwound or slid with respect to each other more than in other base pair steps.

Generating Initial Structures. With proton–proton distance constraints in hand, we then determined eight independent distance geometry (DG) structures as described under Materials and Methods. To measure the similarities between each

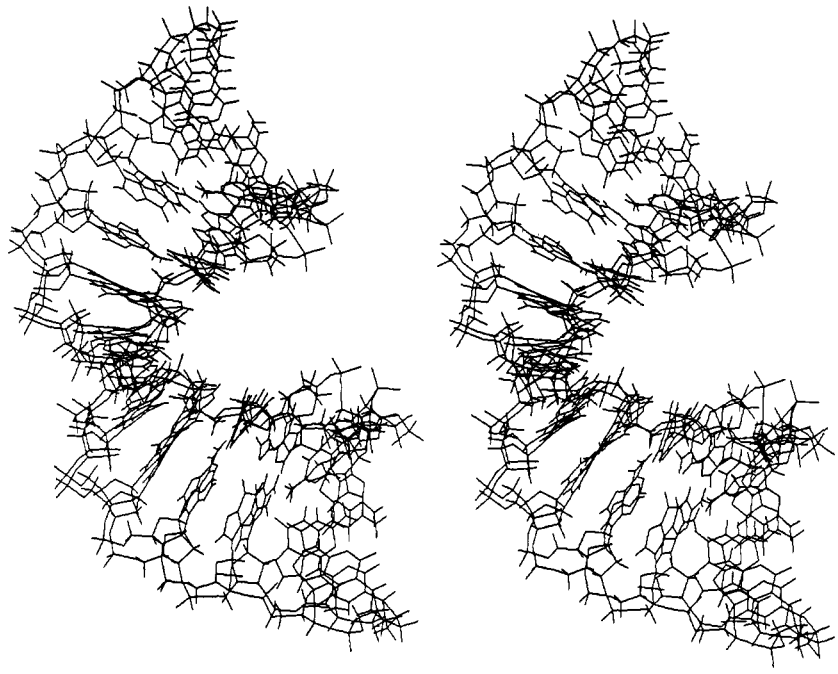

FIGURE 7: Superimposition of two of the eight DG structures of the *Bcl*I dodecamer calculated from distance geometry techniques. Each of these eight initial DG structures was determined from a randomly embedded structure with the distances measured with a two-spin approximation as the distance constraints. The two structures shown superimpose with a RMSD of 1.72 Å.

of the eight refined DG structures, coordinate root-mean-square deviations (RMSD) were calculated for all pairwise combinations of structures. These values varied from 1.6 Å for the best superimposable pair to 2.6 Å for the worst pair. Figure 7 shows stereoviews of two superimposable DG structures whose RMSD values were 1.72 Å. The overall similarity of the two structures, and all other pairs of structures, indicates we have converged to a fairly restricted family of structures, each of which arises from randomly embedded distance constraints. However, as mentioned earlier, the fact that the structures converge to a single family of reasonably superimposable structures does not necessarily mean that we have determined the actual structure. A much more rigorous criterion for the correctness of the structure is that its network of proton coordinates should satisfy the time dependence of the NOESY spectrum. We now routinely perform this back-calculation test for each of the different structures we determine in our laboratory. The advantage of the NOESY back-calculation analysis is that it implicitly utilizes spin diffusion among all proximal proton networks as an added requirement to be satisfied and thus does not depend on the two-spin approximation from which the distances used to construct the initial structure were obtained. Figure 8 shows such a back-calculated NOESY spectrum, presented as stack plots so as not to "hide" unwanted crosspeaks below some contour level. The experimental NOESY spectra (top) and the NOESY spectra back-calculated from the coordinates of a DG structure (center) are shown—the coordinates used are from one of the structures seen in Figure 7. The mixing time for each NOESY is 180 ms, and the two crosspeak regions shown (base H8/H6 to H1′/H5/H3′ and base H8/H6 to H2′R/H2′S/Me) yield information concerning interresidue and intraresidue interproton connectivities. By comparing the two spectra in detail, one should be able to ascertain how well the theoretical NOESY spectrum calculated from the coordinates of the DG structures (created from two-spin approximated distances) matches the actual experimental data and thus obtain an indication of the accuracy of the structure.

Examination of the top two spectra in Figure 8 shows that the experimentally observed NOE's are indeed generated by the DG structure although in some cases the relative NOE intensities are not correct and occasionally they differ markedly from the experimental NOE intensities. A particularly extreme case can be seen near the top-right corner of the left DG plot where H6(2) is obviously much too close to H3′(2)—see Figure 3 for crosspeak identities. In fact, all of the base to H3′(*n*) intensities are somewhat greater than in the experimental data, suggesting that these intraresidue distances are all too short in the DG structure. This strongly suggests that base–H3′(own) distances cannot be obtained reliably by a two-spin approximation; these crosspeaks contain significant intensity contributions from spin-diffusion pathways (probably a base to H2′S to H3′ route), making the measurement of an accurate initial NOE buildup rate impossible for this class of crosspeaks at a mixing rate of 90 ms, the first mixing time where one can reliably integrate these relatively weak crosspeaks. However, the extreme case of the NOE intensity for the H6(2) to H3′(2) crosspeak is much more serious and might be taken to cast doubts on our method of determining structures and/or distances. However, large-scale errors such as this one occur *only* when no distance constraints are input for that particular proton–proton distance due to the presence of partial or severe crosspeak overlaps that prevent measuring individual NOE buildup rates. The distances corresponding to such overlapped crosspeaks are not measured experimentally; they are constrained only by triangulation and thus show the largest deviations from the experimental data—a fact which actually supports the rigor and lack of bias in our method of structure determination since we make no pretense of "knowing" structural constraints if that information is not input as some type of a reliable, experimentally determined, constraint.

Any of the closely related DG structures, though not perfect, can serve as a good starting structure for further refinements. A comparison of the stack plots on the right side of Figure 8 indicates that, with respect to base–H2′R/H2′S crosspeaks, the DG structure appears to be a fairly good representation of a solution structure that satisfies the NOESY data. For

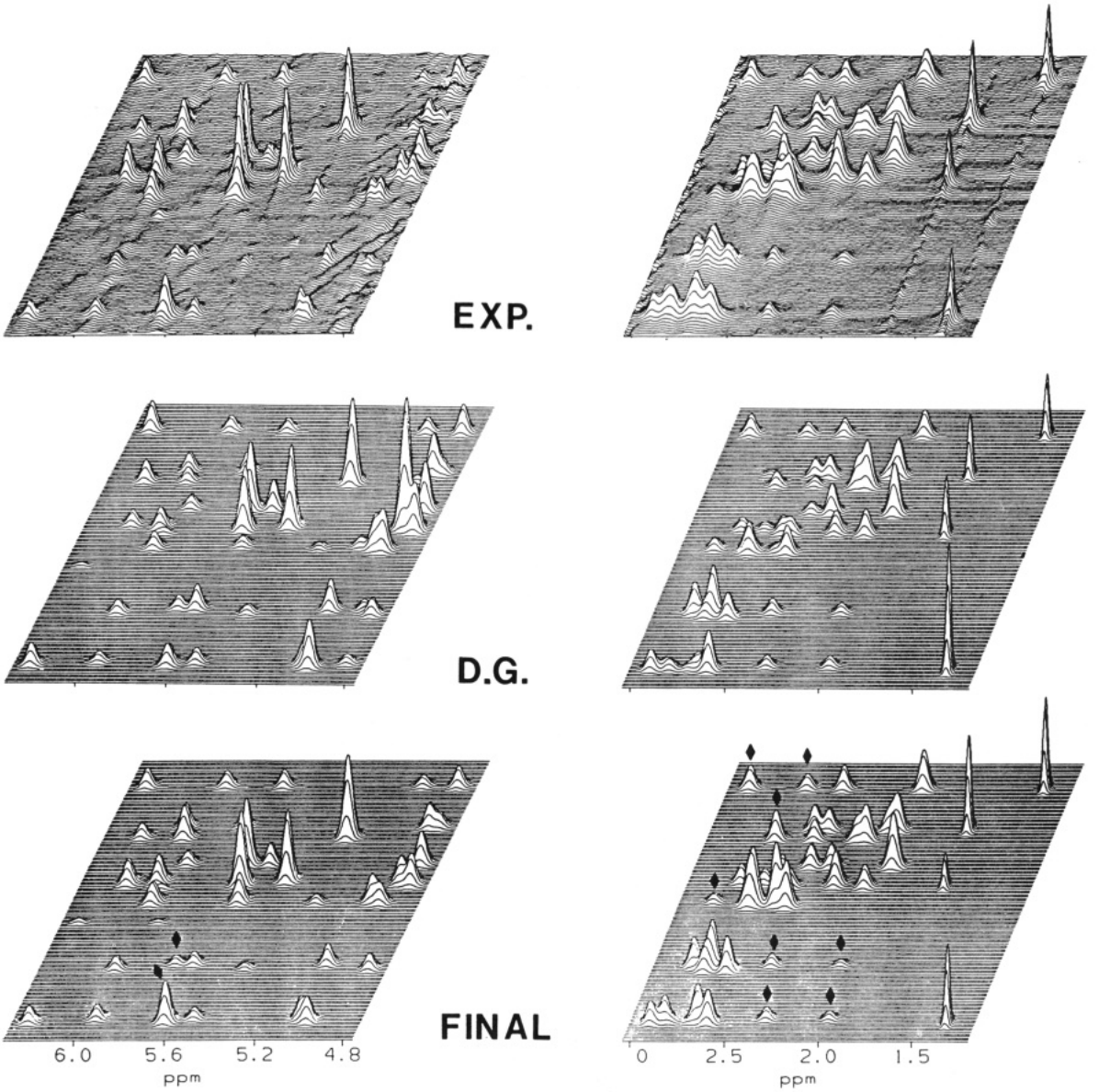

FIGURE 8: Stack plots of two crosspeak regions [base to H1′,H3′ (left) and base to H2′R, H2′S, and methyl (right)] which compare the experimental NOESY spectrum (top), the NOESY spectrum calculated for the DG structure (center), and the NOESY spectrum calculated for FINAL structure (bottom). By comparing the spectra of the DG structure and the FINAL structure, it is seen that protons within the *Bcl*I dodecamer have indeed been moved with respect to each other as discussed in the text. Additionally, by comparing the spectra of the FINAL structure and the experimental spectra, one can see that the match between the two is quite good, indicating we have determined a structure which belongs to the family of structures which satisfy the NOESY data.

most of the crosspeaks in this region, the relative intensities are fairly close to those in the experimental data, reinforcing our confidence that the structure determined with distances measured by the initial rate two-spin approximation is a good starting structure for further refinement. The comparisons presented in Figure 8 show that back-calculating the NOESY spectrum gives a rather detailed assessment of the accuracy of ones structure. This suggests that back-calculation can be an extremely powerful tool for finding errors in interproton distances for structures determined not just by distance geometry but by any technique, including methods based on refining idealized DNA by least-squares and molecular dynamics refinement.

Iterative Back-Calculation and Further Structural Refinement. The back-calculation of the NOESY spectrum of a DG structure at a single mixing time reveals which proton pairs in that structure have severe distance violations with respect to the experimental data. A more quantitative measure for determining interproton distance violations with back-calculation techniques is to compare the time dependence of the experimental and calculated NOE buildup rates for the structure in question. This was performed at 30, 60, 90, 120, 150, and 180 ms, yielding more accurate information about interproton distance violations. The next step in determining a structure which better matches the experimental NOESY data makes use of the distance geometry algorithm DSPACE again. Using DSPACE as a mechanism to move protons, we can shorten the distance between those protons whose NOE buildup rates were too slow (corresponding to proton pairs too far apart) and increase the separation between those proton pairs whose NOE buildup rates were too fast (corresponding to protons too close together). The new interproton distances are then again smoothed against their nearest atoms followed by a smoothing of the upper bounds to improve their bounds. The "temperature" is then raised with the simulated annealing algorithm in order to let the molecule sample the new distance constraints and minimize the deviations from the new distance bounds. During the annealing process, planarity (which forces

the bases to be planar), linearity (which stresses H-bonding), and chirality penalties were turned on. After two cycles of simulated annealing, the resulting structure was refined further with conjugate gradient refinement with the symmetry penalty being added to increase molecular symmetry. The NOESY spectra of this modified structure were then calculated at the appropriate mixing times with BKCALC. Comparisons of the NOE buildup rates between this modified structure and the experimental data were again made, with the level of similarity between the two being determined by visual inspection. Although the match with the experimental spectra was now much better than for the original DG structure, significant deviations were still present (data not shown). Once again, when the NOE buildup rate for a given proton pair was too large or too small, the offending protons were moved apart or closer accordingly. A second back-calculated structure was then generated with DSPACE as described previously, and its NOESY spectra were again back-calculated. After two further cycles of this process, a structure was generated whose NOE buildup rates at six mixing times did not deviate significantly from the experimentally observed NOE buildup rates.

At this point, even though the match between the experimental NOESY's and the back-calculated NOESY's was quite good, an additional series of simulated annealing cycles were performed. During these cycles, a Lennard–Jones potential for van der Waals was added to the refinement constraints. The motivation behind adding this potential to the constraints comes from the observation that distance geometry tends to determine slightly expanded structures. By adding the attractive Lennard–Jones potential to our constraints, we had hoped to "tighten up" or compact our DNA structure. The power of these further refinements was observed after the NOESY back-calculation of the resulting structure when several new NOE's between previously distant protons were observed. This allowed us to add several new lower bounds constraints to push these protons apart since their NOE's were not observed in the experimental spectra. After the series of iterative refinements with the Lennard–Jones potential turned on, a structure whose back-calculated NOESY spectra matched the experimental data quite well was determined (this was called the FINAL structure). Figure 8 compares two regions of the NOESY spectrum at 180 ms for the experimental data (top), the DG structure (center), and the FINAL structure (bottom). It is readily apparent by comparing the NOESY spectra for the DG structure (center) and the FINAL structure (bottom) that we have significantly changed the structure of the *Bcl*I dodecamer during the iterative back-calculation refinement. In addition, one should notice that the overall match between the experimental NOESY data (top) and the calculated NOESY data corresponding to the FINAL structure (bottom) is quite good. In particular, the FINAL structure faithfully reproduces the anomalously strong H8(6)–H1′(5) crosspeak and the anomalously weak H8(5)–H1′(4) crosspeak (designated by diamonds in the bottom-left panel: also see Figure 3) observed in the experimental data. On the right side of Figure 8, the experimental data and the FINAL data also match well in the H8/H6 to H2′R/H2′S(n,n − 1) crosspeak region. The FINAL structure shows very weak base–H2′R/H2′S(n − 1) crosspeaks for the A9-T8, G5-T4, and G10-T9 steps but much stronger crosspeaks for the base–H2′R/H2′S(n − 1) steps for T7-A6 and C12-G11, as does the experimental data; these peaks are designated by diamonds in Figure 8—see also Figure 2. The experimental NOESY spectra and the theoretical NOESY spectra calculated for the FINAL structure match well at the 180-ms mixing time, indicating that we have indeed determined a structure rather close to the solution structure. However, an even truer test of the accuracy of the structure can be ascertained by comparing the time course of both the experimental and back calculated NOESY spectra, since it is the NOE buildup rates, not the intensity at a single intermediate mixing time, which yields quantitative distance information. Figures 9 and 10 show the experimental NOESY spectra and the theoretical NOESY spectra calculated from the coordinates of the FINAL structure at five earlier mixing times for the two crosspeak regions discussed in depth previously. Some characteristics of the NOE time courses which bear mentioning include the observation of spin diffusion (nonlinear crosspeak growth rates) for protons close in space. In particular, all the strong aromatic base to H2′S crosspeaks (see assignment table) seen in Figure 10 already show spin-diffusion effects by 60 ms. A second characteristic of the NOE time course worth discussing is the similarity between the experimental and theoretical spectra for both strong and weak crosspeaks, indicating that BKCALC works correctly and demonstrating that the structure which we have determined matches the experimental data well. The results show that we have succeeded in producing a set of atomic coordinates for the *Bcl*I dodecamer that satisfy the bond lengths and bond angles of standard nucleotide chemistry and in which the interproton spatial arrangement satisfies the observed multiple proton network of dipolar cross-relaxation pathways.

Figure 11 shows the three-dimensional structure for the T4-G5-A6-T7 base pair region and demonstrates the level of determination for the FINAL *Bcl*I dodecamer structure. In this figure, we have connected some of the experimentally measured interresidue proton–proton distances (base to base and base to sugar) by solid lines. By comparing the separation between any pair of protons in the FINAL structure to their corresponding NOE buildup rates, we find that the dodecamer structure is entirely consistent with the NOESY data. In addition, for each base pair step, at least four accurately measured interresidue constraints (neglecting the fact that the absences of NOE's are also lower bound constraints) were measured, indicating a more than satisfactory level of interresidue structural determination has been obtained. For example, the A6 to T7 base pair step has eight interresidue constraints which were measured, suggesting that the local structure for the A6-T7 junction must indeed be very accurate. An overdetermination of constraints such as this is consistently found throughout the structure of the conserved recognition sequence, indicating that the nearest-neighbor helical steps must be quite accurate representations of the actual structure. When analyzed in fine detail, the local structure "anomalies", i.e., NOE intensities present in the experimental data but not expected in classical idealized B-DNA, are all faithfully duplicated in the FINAL structure. In particular, the very short distance between the H8 of A6 and the H1′ of G5, in conjunction with the longish distance between the base proton of G5 and its own H1′ and coupled with the longer distance from G5 H8 to the H1′ of T4, is a configuration contained within the structure. These proton–proton distances were predicted to occur at the level of initial interproton distance measurements [see Figures 3, 9, and 10 for the H8 to (n − 1) H1′ intensities for A6 and G5]. We therefore feel that there is high probability that we have determined the structure of this duplex in solution. However, whether we have or not, these results demonstrate the current limit of rigorous application of distance geometry and NOESY simulation in determining

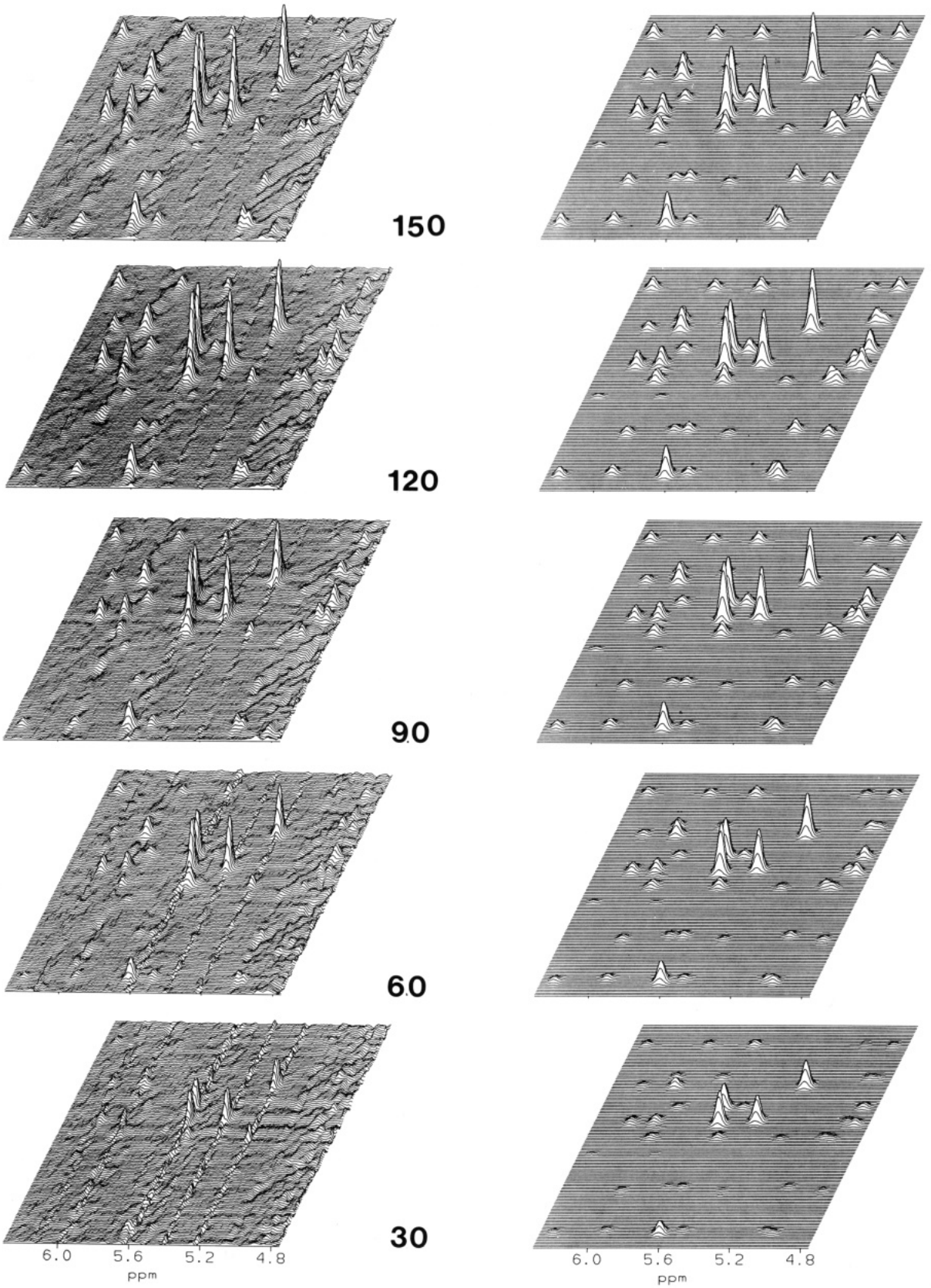

FIGURE 9: Stack plots of the aromatic base to H1′,H3′ crosspeak region which compare the NOE growth rates, at six mixing times, for the experimental NOESY spectra and the NOESY spectra calculated with the FINAL structures proton coordinates. The good compatibility of the two spectra suggests we have determined a structure close to the actual solution structure.

the three-dimensional solution structure of DNA without ad hoc model building. Additionally, analysis of specific interproton distances in the BKCALC-refined FINAL structure that recreates the NOESY time dependence, compared to the two-spin initial rate estimates of those same distances, reveals that certain types of distances are systematically underestimated in the two-spin approximation, even at 30-ms mixing times; however, by use of known model test systems, this "foreshortening" due to spin diffusion through intervening spins is corrected in the BKCALC refinement (Banks and Reid, un-

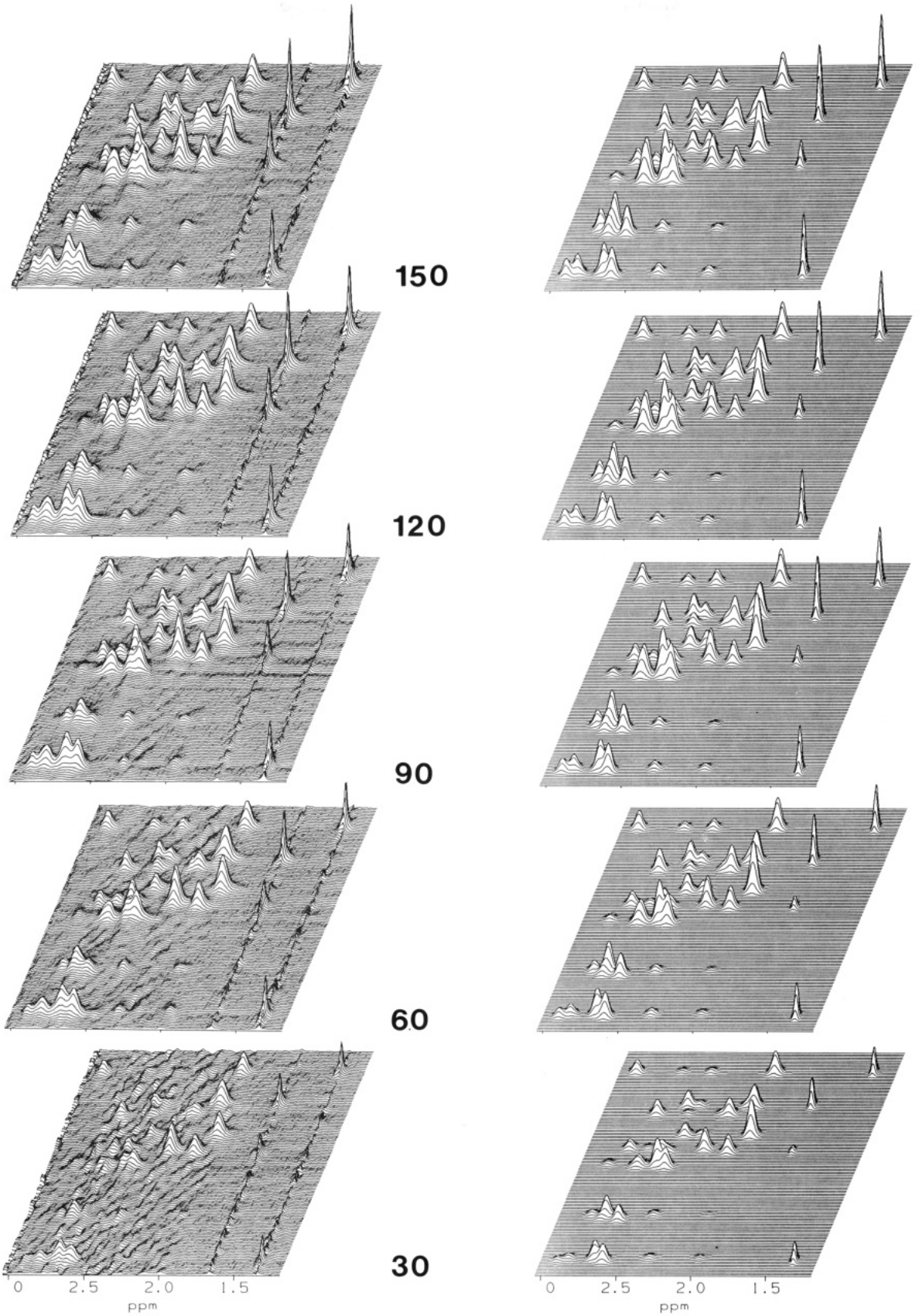

FIGURE 10: Stack plots of the aromatic base to H2′R, H2′S, and methyl crosspeak region which compare the NOE growth rates, at six mixing times, for the experimental NOESY spectra and the NOESY spectra calculated with the FINAL structure proton coordinates.

published results).

SUMMARY

The three-dimensional structural determination of short DNA sequences using distance geometry and NOESY spectrum back-calculation refinement is a technique that yields experimentally consistent, though somewhat unusual, structures for the *Bcl*I dodecamer—the FINAL structure of the conserved recognition sequence (TGATCA) can be seen in Figure 12. Other solution structures for DNA that are

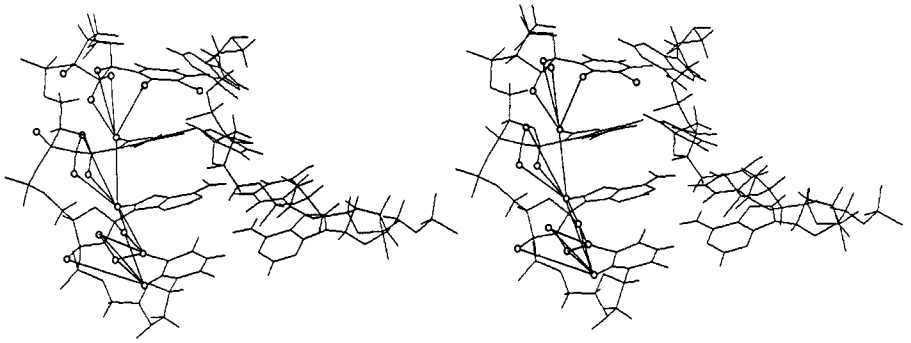

FIGURE 11: Stereo figure of T4-G5-A6-T7 region for the FINAL *Bcl*I structure. The solid lines connect the experimentally measured interresidue proton–proton distances, showing that the amount of determination present is more than enough to accurately determine local structural geometries. In addition, the structure shown contains the expected proton–proton distance ratios for the H8(A6)–H1′(G5), H8(G5)–H1′(G5), and H8(G5)–H1′(T4) distances as predicted during the initial distance measurement phase of the structural determination process. The match between the NOE buildup rates calculated for this structure and that measured experimentally again indicates that this particular region is very well determined.

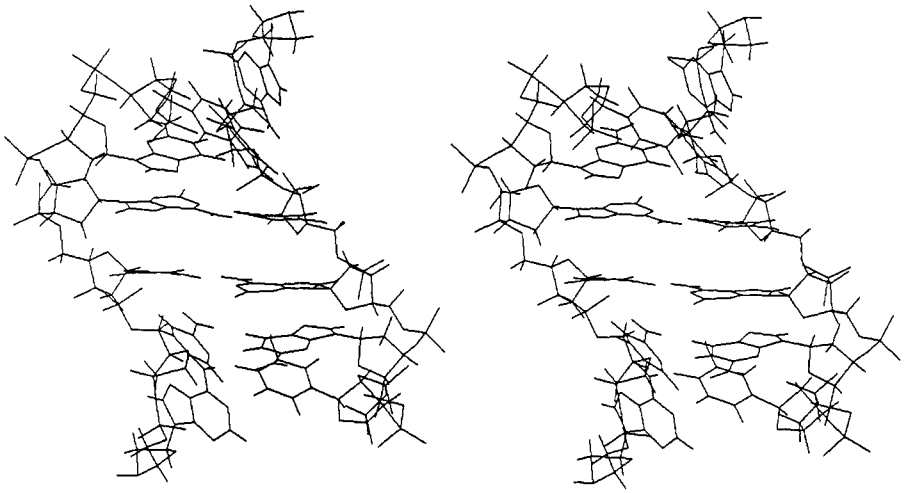

FIGURE 12: Stereo figure of the conserved recognition sequence (T4-G5-A6-T7-C8-A9) as determined for the FINAL *Bcl*I dodecamer structure.

somewhat less "abnormal" have been determined in this laboratory for the *Hgi*I, *Eco*RI, and *Eco*RV restriction sequences with exactly the same methods (unpublished results); compared to these more "normal" structures, the *Bcl*I duplex is certainly a rather "unusual" DNA structure. However, it is worth noting that normal and abnormal are subjective judgements biased by text book models of idealized average DNA reconstructed from fiber diffraction data which, by definition, prohibits sequence-dependent variation in local structure. As a test to determine whether the algorithm generates accurate structures with distances from known structural coordinates, other members of this laboratory have demonstrated that, using idealized DNA distances, DSPACE does in fact regenerate idealized B-form DNA from input distance constraints similar to those typically measured (unpublished results). Therefore, it appears that the information that defines the peculiar *Bcl*I dodecamer structure lies within the experimentally measured distances, and the peculiarity of the structure is not the result of faults in the distance geometry algorithm. A detailed comparison of the experimental NOE buildup rates and the theoretical NOE buildup rates calculated from the coordinates of the FINAL structure shows that they coincide very well, suggesting that our input distance constraints have been measured as accurately as possible with the data at hand. It may therefore be concluded that the *Bcl*I dodecamer structure has been determined as precisely as possible with the NOESY distance data and the structure must be close to the actual solution structure. Accordingly, we feel that the details of the structure itself might yield insights into the ability of this particular sequence to be recognized by the *Bcl*I restriction endonuclease. In this connection, we note with interest that the single-crystal structure of the *Eco*RI restriction sequence GAATTC shows marked local deviations in twist, slide, and propeller twist (Dickerson & Drew, 1981) and that the X-ray structures of some operator DNA sequences complexed to their repressors are quite abnormal (Anderson et al., 1987; Otwinowski et al., 1988).

Description of the structure, shown in Figure 12, in terms of the usual helical DNA parameters presents somewhat of a problem. In particular, accurate measurements of the various interbase parameters related to the helix axis (i.e., roll) proved to be virtually impossible due to the large amount of curvature for the structure which made it impossible to define a global helical axis. Without an accurately determined global helical axis, the description of tilt, roll, and twist parameters with respect to the helix axis is meaningless. In addition, until a consensus is reached on how to define the local structure of abnormal DNA (Dickerson, 1989; Bhattacharyya & Bansal, 1989; Lavery & Sklenar, 1989), an in-depth analysis of the various local interbase parameters would again provide potentially irrelevant structural information. Therefore, at this point in time, only a brief description of a few of the relevant interbase structural parameters and distance separations will be presented (Table III); atomic coordinates will be provided upon request.

The most obvious structural peculiarity which can be found is the large amount of roll observed between the bases of C8 and T7. The presence of such a large roll for this particular

Table III: Structural Parameters for the *BclI* Duplex FINAL Structure

residue	glycosyl χ (deg)	pseudorotation angle (deg)	sugar conformation
G1	−106	172	C2′-endo–C3′-exo
C2	−128	174	C2′-endo–C3′-exo
C3	−142	178	C2′-endo–C3′-exo
T4	−90	174	C2′-endo–C3′-exo
G5	−50	171	C2′-endo–C3′-exo
A6	−119	177	C2′-endo–C3′-exo
T7	−137	143	C2′-endo–C1′-exo
C8	−125	160	C2′-endo
A9	−105	168	C2′-endo
G10	−69	160	C2′-endo
G11	−96	124	C1′-exo
C12	−116	141	C1′-exo–C2′-endo

base pair step was not suggested by our preliminary data analysis as no anomalous NOE's between protons on these two residues were observed. Furthermore, this particular base pair step is probably one of the most overdetermined steps in the sequence because the base, 1′, 2′, and 2″ protons are all well resolved for both residues. However, an examination of the intraresidue structural parameters for both T7 and C8 strongly suggests the presence of a marked structural deviation from B-like DNA at this base pair step. The glycosyl torsion angle (χ), defined as the O4′–C1′–N1–C2 angle for pyrimidines and the O4′–C1′–N9–C4 angle for purines, yields information concerning the rotation of the base with respect to the sugar. For idealized B-form DNA, the χ angle is measured to be −101°, and as can be seen in Table III, the χ angle for T7 deviates more from ideal B-form DNA (containing more anti character) than the χ angles for the other residues in the conserved recognition sequence. This fact, coupled with the somewhat unusual C2′-endo–C1′-exo sugar conformation for T7 (see Table III), places constraints on the ability of this particular residue to conform to a classical B-form structure, possibly creating the roll observed with respect to C8. However, the fact that the A6-T7 base pair step appears to be fairly "normal" indicates that whatever structural constraints are present within T7, as suggested by the χ and pseudorotation angles, these effects are only observed on the base pair step in the 3′ direction.

Further analysis of the structure seen in Figure 12 shows a structural aberration within the T4-G5-A6 base pair steps. This particular bent region of the duplex contains low χ angles required to accommodate the anomalous interresidue proton–proton distances measured and discussed previously. The low χ angle (indicating the presence increasing syn character) for G5 was necessitated by the measured interproton distance of 4.1 Å for the G5 H8 to G5 H1′, a separation that is significantly larger than other H8/H6 to H1′ distances. Because intervening spins tend to increase the NOE and foreshorten the apparent distance, this already long distance can be taken as a lower estimate. It follows that there should be a relatively large amount of base ring twist with respect to the sugar for this base as the base H8 is forced to turn away from the sugar H1′ proton as can be seen in Figure 12. It is this abnormal base–sugar rotation into the high-anti (–sc) range which is partially responsible for observed bend, due in part to the roll it causes between the aromatic rings of G5 and A6. Since the χ angle for A6 is −119°, an angle which produces a shorter base to H1′ distance and a more B-like base, it becomes impossible to stack the aromatic rings of G5 and A6 while still maintaining their C2′-endo–C3′-exo sugar conformations, and hence, the two bases must roll with respect to each other to form the conformation that matches the NOESY data.

In summary, the *BclI* restriction site DNA is bent, and it is possible that this curvature (due to interbase rolling) is necessary for the recognition and cleavage of the *BclI* restriction dodecamer by the *BclI* restriction endonuclease. A definitive statement on the biological relevance of this curvature in the recognition process must await structural studies on the nuclease–DNA complex and on the effects of replacing G5 with other nucleotides.

References

Anderson, J. E., Ptashne, M., & Harrison, S. C. (1987) *Nature 326*, 846–852.

Aue, W. P., Bartholdi, E., & Ernst, R. R. (1976) *J. Chem. Phys. 64*, 2229–2246.

Bartholdi, E., & Ernst, R. R. (1973) *J. Magn. Reson. 11*, 9–19.

Berg, O. G., & Blomberg, C. (1978) *Biophys. Chem. 8*, 271–280.

Berg, O. G., Winter, R. B., & von Hippel, P. H. (1981) *Biochemistry 20*, 6929–6948.

Bhattacharyya, D., & Bansal, B. (1989) *J. Biomol. Struct. Dyn. 6*, 635–654.

Bingham, A. H. A., Atkinson, T., Sciaky, D., & Roberts, R. J. (1978) *Nucleic Acids Res. 5(10)*, 3457–3467.

Bothner-By, A. A., & Noggle, J. H. (1979) *J. Am. Chem. Soc. 101*, 5152–5153.

Bundi, A., & Wüthrich, K. (1979) *Biopolymers 18*, 285–297.

Bystrov, V. F. (1976) *Prog. Nucl. Magn. Reson. Spectrosc. 10*, 41–81.

Chou, S.-H., Wemmer, D. E., Hare, D. R., & Reid, B. R. (1984) *Biochemistry 23*, 2257–2262.

Clore, G. M., & Gronenborn, A. M. (1983) *EMBO J. 2*, 2109–2115.

Clore, G. M., & Gronenborn, A. M. (1985a) *FEBS Lett. 179*, 187–198.

Clore, G. M., & Gronenborn, A. M. (1985b) *EMBO J. 4*, 829.

Crippen, G. M. (1977) *J. Comput. Phys. 24*, 96–104.

Dickerson, R. E. (1989) *J. Biomol. Struct. Dyn. 6*, 627–634.

Dickerson, R. E., & Drew, H. R. (1981) *J. Mol. Biol. 149*, 761–785.

Drew, H. R., & Travers, A. A. (1984) *Cell (Cambridge, Mass.) 77*, 491–502.

Drew, H. R., & Travers, A. A. (1985) *J. Mol. Biol. 186*, 773–790.

Hare, D. R., & Reid, B. R. (1986) *Biochemistry 25*, 5341–5350.

Hare, D. R., Wemmer, D. E., Chou, S.-H., Drobny, G., & Reid, B. R. (1983) *J. Mol. Biol. 171*, 319–336.

Hare, D. R., Shapiro, L., & Patel, D. J. (1986a) *Biochemistry 25*, 7445–7456.

Hare, D. R., Shapiro, L., & Patel, D. J. (1986b) *Biochemistry 25*, 7456–7464.

Havel, T. F., & Wüthrich, K. (1984) *Bull. Math. Biol. 46*, 673–698.

Havel, T. F., & Wüthrich, K. (1985) *J. Mol. Biol. 182*, 281–294.

Havel, T. F., Crippen, G. M., & Kuntz, I. D. (1979) *Biopolymers 18*, 73–81.

Havel, T. F., Kuntz, I. D., & Crippen, G. M. (1983a) *Bull. Math. Biol. 45*, 665–720.

Havel, T. F., Kuntz, I. D., & Crippen, G. M. (1983b) *J. Theor. Biol. 104*, 383–400.

Hull, W. A., & Sykes, B. D. (1975) *J. Chem. Phys. 63*, 867–880.

Kalk, A., & Berendsen, H. J. D. (1976) *J. Magn. Reson. 24*, 343–366.

Kintanar, A., Klevit, R. E., & Reid, B. R. (1987) *Nucleic Acids Res. 14(15)*, 5845-5862.
Kline, A. D., & Wüthrich, K. (1986) *J. Biol. Chem. 192*, 869-890.
Kumar, M. R., Wagner, G., Ernst, R. R., & Wüthrich, K. (1981) *J. Am. Chem. Soc. 103*, 3654-3658.
Lavery, R., & Sklenar, H. (1989) *J. Biomol. Struct. Dyn. 6*, 655-667.
Lefèvre, J.-F., Lane, A. N., & Jardetzky, O. (1987) *Biochemistry 26*, 5076-5090.
Lomonossoff, G. P., Butler, P. J. G., & Klug, A. (1981) *J. Mol. Biol. 149*, 745-760.
Macura, S., & Ernst, R. R. (1980) *Mol. Phys. 1*, 95-117.
Nerdal, W., Hare, D. R., & Reid, B. R. (1988) *J. Mol. Biol.* (in press).
Nigles, M., Clore, G. M., Gronenborn, A. M., Brunger, A. T., Karplus, M., & Nillson, L. (1987a) *Biochemistry 26*, 3718-3733.
Nigles, M., Clore, G. M., Gronenborn, A. M., Piel, N., & McLaughlin, L. W. (1987b) *Biochemistry 26*, 3734-3744.
Noggle, J. H., & Schirmer, R. E. (1971) *The Nuclear Overhauser Effect*, Academic, New York.
Ohlendorf, D. H., & Matthews, B. W. (1983) *Annu. Rev. Biophys. Bioeng. 12*, 259-284.
Otting, G., Widmer, H., Wagner, G., & Wüthrich, K. (1986) *J. Magn. Reson. 66*, 187-193.
Otwinowski, Z., Schevitz, R. W., Zhang, R.-G., Lawson, C. L., Jaudimick, R. O., Marmorstein, B. F., & Sigler, P. B. (1987) *Nature 335*, 321-329.
Rance, M., Sørenson, O. W., Bodenhausen, G., Wagner, G., Ernst, R. R., & Wüthrich, K. (1983) *Biochem. Biophys. Res. Commun. 117*, 479-485.
Redfield, A. G. (1978) *Methods Enzymol. 49*, 253-270.
Rhodes, D. R. (1982) in *Topics in Nucleic Acids Structures* (Neidle, S., Ed.) Part 2, pp 287-304, MacMillen, London.
Scheek, R. M., Russo, N., Boeleus, R., Kaptein, R., & van Boom, J. H. (1983) *J. Am. Chem. Soc. 105*, 2914-2916.
Shakked, Z., Rabinovich, D., Kennard, D., Cruse, W. B. T., Salisbury, S. A., & Viewamitra, A. (1983) *J. Mol. Biol. 166*, 183-201.
States, D. J., Haberkorn, R. A., & Ruben, D. J. (1982) *J. Magn. Reson. 48*, 286-292.
Takeda, Y., Kin, J. G., Caday, C. B., Steers, E., Jr., Ohlendorf, D. H., Anderson, W. F., & Matthews, B. W. (1986) *J. Biol. Chem. 261*, 8608-8616.
Tropp, J., & Redfield, A. G. (1981) *Biochemistry 20*, 2133-2140.
von Hipple, P. H., & McGhee, J. D. (1972) *Annu. Rev. Biochem. 41*, 231-300.
Wagner, G., & Wüthrich, K. (1979) *J. Magn. Reson. 33*, 675-680.
Weber, P. L., Wemmer, D. E., & Reid, B. R. (1985) *Biochemistry 24*, 4553-4562.
Weber, P. L., Brown, S. C., & Mueller, L. (1987) *Biochemistry 26*, 7282-7290.
Wemmer, D. E., Chou, S.-H., & Reid, B. R. (1984a) *J. Mol. Biol. 180*, 41-60.
Wemmer, D. E., Chou, S.-H., Hare, D. R., & Reid, B. R. (1984b) *Biochemistry 23*, 2262-2268.
Williamson, M. P., Havel, T. F., & Wüthrich, K. (1985) *J. Mol. Biol. 182*, 295-315.

Microtubules Accelerate ADP Release by Dynein†

Erika L. F. Holzbaur and Kenneth A. Johnson*
Department of Molecular and Cell Biology, 301 Althouse Laboratory, The Pennsylvania State University, University Park, Pennsylvania 16802

Received November 29, 1988; Revised Manuscript Received April 26, 1989

ABSTRACT: The effects of microtubules on the phosphate–water oxygen exchange reactions catalyzed by dynein were examined in order to determine the mechanism by which microtubules activate the ATPase. Microtubules inhibited the rate of medium exchange observed during net ATP hydrolysis. Inhibition of the exchange reaction was proportional to the extent of microtubule activation of ATP turnover with no effect on the partition coefficient. These data argue that microtubules do not increase the rate of release of phosphate from dynein; rather, they increase the rate of ADP release. Microtubules markedly inhibited medium phosphate–water exchange reactions observed in the presence of ADP and P_i. With increasing concentrations of ADP, the rate of exchange increased in parallel to the dissociation of dynein from the microtubules, suggesting that only free dynein and not the microtubule–dynein complex catalyzes the exchange reaction. The rates of dynein binding to microtubules in the absence and presence of saturating ADP were 1.6×10^6 and 9.8×10^5 M^{-1} s^{-1}, respectively. ADP inhibited the rate of the ATP-induced dissociation of the microtubule–dynein complex with an apparent K_d = 0.37 mM for the binding of ADP to the microtubule–dynein complex. However, the rate of dissociation of ADP from the M·D·ADP complex was quite fast ($\sim$1000 s^{-1}). These data support the postulate of a high-energy dynein–ADP intermediate and indicate that microtubules activate the dynein ATPase by enhancing the rate of ADP release.

Dynein couples the energy of ATP hydrolysis to drive the sliding of adjacent microtubule doublets in the axonemes of eukaryotic cilia and flagella [for reviews, see Gibbons (1981) and Johnson (1985)]. Pre-steady-state kinetic studies have defined the first two steps of the crossbridge cycle for the microtubule–dynein ATPase (Porter & Johnson, 1983b; Johnson, 1983). In Scheme I, which is similar to the Lymn–Taylor scheme for actomyosin (Lymn & Taylor, 1971; Taylor, 1979), the binding of ATP induces the dissociation of the

†This work was supported by NIH Grant GM26726 to K.A.J. K.A.J. was supported by an Established Investigatorship from the American Heart Association with funds contributed in part by the Pennsylvania Affiliate.
*Author to whom correspondence should be addressed.

0006-2960/89/0428-7010$01.50/0